Q. J. R. Meteorol. Soc. (1988), **114**, pp. 1385–1409 551.513.1:551.587(215–13)"32"

The seasonal evolution of planetary waves in the southern hemisphere stratosphere and troposphere

By WILLIAM J. RANDEL

National Center for Atmospheric Research, Boulder, U.S.A.*

(Received 17 September 1987; revised 2 March 1988)

SUMMARY

Seasonality in planetary wave structure in the southern hemisphere stratosphere and troposphere (1000–1 mb) is studied based on eight years (1979–1986) of daily geopotential data. Emphasis is placed on the distinctive seasonality in the stratosphere, along with tracing the stratospheric fluctuations into the troposphere. Time filtering is used to separate stationary and transient components. Maximum geopotential height variance is observed in the middle to upper stratosphere in late winter–spring, with a distinct secondary, smaller maximum in late fall–early winter; these maxima sandwich the strongest mid-winter zonal winds. This sequence occurs approximately one month earlier in the upper stratosphere. Two corresponding peaks are observed in stratospheric zonal mean wind and temperature fluctuations. The two maxima in stratospheric wave variance are not in agreement with observed seasonal changes in quasi-geostrophic refractive index of the zonal mean flow.

The stratospheric geopotential variance maxima result from nearly equal amounts of stationary and transient zonal wave-1 fluctuations, with transient wave 2 also contributing during late winter. Stationary wave 1 shows intriguing seasonal evolution: the early winter maximum is predominantly equivalent barotropic, whereas that of late winter–spring is highly baroclinic in the stratosphere. Stratospheric poleward fluxes of heat and momentum both exhibit pronounced maxima during September–October; these result primarily from the stationary wave-1 contributions, and the transients assume a secondary role. Although not as pronounced as the stationary wave seasonality, seasonal differences in transient wave behaviour are also documented, including three-dimensional propagation characteristics and wave–mean flow interaction diagnostics.

1. INTRODUCTION

A significant portion of the spatial and temporal variability of the atmosphere is contained in planetary-scale motions. While such large-scale features clearly dominate the winter stratosphere, planetary wave variability is also important in the troposphere, where it has been connected with blocking (Quiroz 1987), persistent weather regimes (Hansen and Sutera 1986), and storm track variability (Lau 1988). Additionally, although predictability studies suggest that the highest forecast skill should be found for planetary-scale motions, actual forecast experiments show substantial errors, suggesting that the dynamics of planetary waves are not completely understood (see, e.g., Baumhefner 1984). Further study of planetary waves is thus warranted, and because a substantial fraction of tropospherically generated planetary waves propagates into the stratosphere during winter, knowledge of their structure and evolution throughout both regions is important. Furthermore, analysis of planetary wave behaviour in the southern hemisphere (SH) may yield insight because forcing mechanisms are distinctive from those in the northern hemisphere, in addition to there being substantially different climatologies. Finally, such analyses provide verification data for a host of model studies.

The initial motivation for this study was to document the strong seasonal variation in stationary waves in the SH stratosphere. Previous observational analyses of SH stationary stratospheric waves (van Loon and Jenne 1972; van Loon *et al.* 1973; Hartmann 1977), along with the more recent analyses of Hartmann *et al.* (1984) and Randel (1987a), pointed out that during the SH *winter* (June–August) stationary waves are weaker than the transient components and characterized by an equivalent barotropic vertical structure.

* The National Center for Atmospheric Research is sponsored by the National Science Foundation.

In contrast to this situation, the stationary waves in the stratosphere during SH *spring* (September–November) are strongly baroclinic, contributing by far the largest poleward heat and momentum fluxes during this time, and the transient waves assume a secondary role. The purpose here is to document this strong seasonality; in particular, the stationary wave development throughout the troposphere and stratosphere is studied in conjunction with seasonal changes in the zonal mean flow and transient waves. Results are compared with the better documented seasonal variations in the NH, and discussed in light of current theories. Furthermore, the tropospheric stationary waves in the present data are compared with those reported in van Loon and Jenne (1972), Trenberth (1980) and Karoly (1985), those being from different time samples and analysis procedures.

The seasonally-varying behaviour of transient planetary waves is also studied here, revealing characteristics distinct from those of the stationary waves. Zonal propagation is studied via the modified time-lag correlation diagrams of Fraedrich and Lutz (1987), revealing eastward phase progression throughout the stratosphere for all months, along with eastward group velocity during late winter–spring. Vertical and meridional propagation is analysed via the modified longitude–time-lag correlation diagrams of Randel (1988). Distinctive signatures are found during early and late winter, although the stratospheric fluctuations can be clearly traced into the troposphere for all months. Observed changes in transient wave characteristics are discussed in light of the stationary wave and zonal flow evolution. A major strength of this study is the length of the data base analysed (eight years); ensemble statistics provide high quality estimates of seasonal variations throughout the troposphere and stratosphere.

2. Data and analysis techniques

(*a*) *Data*

The data used in this study are daily hemispheric geopotential height grids from 1000–1 mb archived at NCAR. Data for 100 mb and below are 12 UTC National Meteorological Center (NMC) operational analyses, while grids at 70 mb and above are from daily analyses made at the Climate Analysis Center, anchored on the 100 mb NMC data. These are the same type of data analysed by Hartmann *et al.* (1984) and Geller *et al.* (1983), among other recent studies. Trenberth and Olson (1988) have recently studied the quality of NMC analyses over 1000–100 mb during this period, noting modifications to the analysis scheme and quality changes in the resultant data. Their analyses show the largest impact of such changes to occur in the tropics, and for fields such as relative humidity; the impact on extratropical height analyses, particularly planetary-scale features, is probably smaller. Karoly (1987) has studied SH stratospheric circulation statistics (similar to those used here) derived using stratospheric thickness data anchored to three different 100 mb analyses; he finds the results to be qualitatively insensitive to the exact lower-level data used, especially for time-averaged fields. Details of the stratospheric geopotential analyses, along with various changes in operational satellites and analysis schemes over 1979–1986, are discussed in Gelman *et al.* (1986). An extensive global climatology based on these data, including means and estimates of daily and interannual variabilities, along with discussions on the data origin, quality, and processing is available in Randel (1987c).

The data studied here are daily global analyses for the years 1979–1986, although primary attention is focused on the SH winter months March to November. The geopotential grids have been harmomically analysed for analyses based on zonal wavenumber. Poleward fluxes of heat and momentum are evaluated using winds derived via the linearized zonal and meridional momentum equations, subject to singularity

constraints, as discussed in Randel (1987b); such analyses are superior to local geostrophic values in the stratosphere. Similar wind analyses were used by Robinson (1986a) and Hitchman *et al.* (1987). The zonal mean gradient approximation is used to evaluate zonal mean winds, and values are linearly interpolated over 2°S–20°N (as discussed in Randel (1987c)). Eliassen–Palm (EP) flux divergences are calculated from the primitive equation expressions, neglecting terms involving the vertical velocity. EP flux vectors are scaled with the inverse square root of density, to make them visible throughout the stratosphere.

(*b*) *Dynamic time scales—stationary and transient waves*

The predominant variability in the SH stratosphere is on the seasonal time scale, because the intense mid-winter polar vortex is disturbed relatively little by planetary wave activity. The amount of planetary wave variance is also predominantly seasonally dependent. Figures 1(a,b) show stratospheric power spectra of 10 mb zonal mean wind and 10 mb wave 'amplitude' (square root of wave variance) averaged over 50°–60°S, calculated from daily time series over March–November, and averaged over the eight

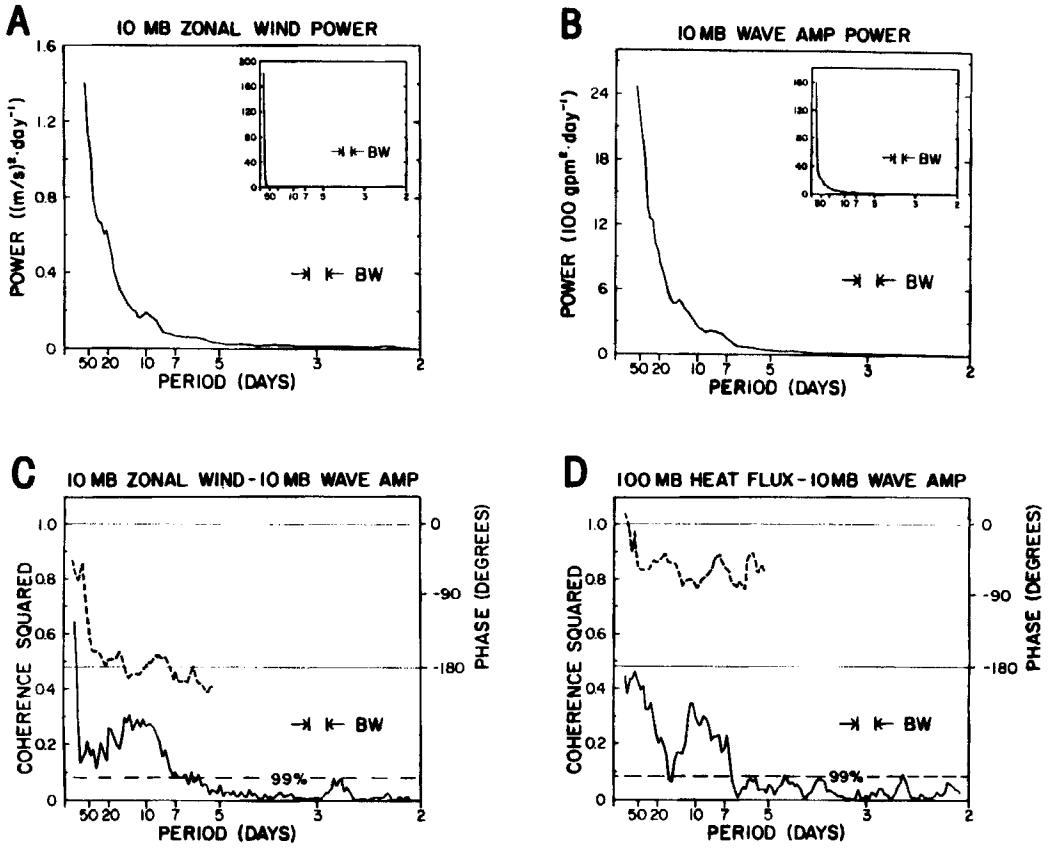

Figure 1. Power spectra of (a) 10 mb zonal mean wind, and (b) 10 mb wave 'amplitude' (square root of variance), calculated from daily data (March–November) over 50°–60° and averaged over 1979–86. Also shown are coherence squared (solid lines) and phase spectra (dashed lines) between (c) 10 mb zonal mean wind and 10 mb wave amplitude, and (d) 10 mb wave amplitude and 100 mb heat flux. The lowest frequency spectral estimates in (a) and (b) are not plotted in the main diagram due to their size, but included in the inset (the ordinate is the same as the main figures). The 99% limit for a null hypothesis of zero coherence is indicated in the lower figures, and a negative phase difference indicates zonal wind or heat flux leading wave amplitude. The spectral bandwidth is indicated in each figure.

years 1979–1986. Both spectra show a complete dominance of power in the lowest frequency (seasonal) range; the zonal wind and wave amplitude spectra contain greater than 98 and 80% of their power, respectively, in periods greater than 30 days. Beyond the seasonal time scale these spectra show significant power in the 30- to 5-day period range, with negligible high-frequency (>5 day) contributions.

Significant dynamical time scales in the stratosphere are revealed by coherent fluctuations of the system. Figure 1(c) shows the coherence and phase spectra between zonal mean wind and wave amplitude fluctuations at 10 mb, while Fig. 1(d) illustrates similar calculations between 10 mb wave amplitude and 100 mb heat flux (with all quantities averaged over 50°–60°S). Values of the coherence squared and phase in Figs. 1(c,d) are averaged over six adjacent spectral estimates and eight years of data, resulting in 48 degrees of freedom (df); the 99% limit for a null hypothesis of zero coherence for 48 df is 0·094 (Jenkins and Watts 1968). Significant coherence is found in both Figs. 1(c,d) for periods greater than about seven days, with two relative maxima in the coherence spectra at periods near 7–15 days and at low (seasonal) frequencies. The phase spectra reveal an out-of-phase relationship between wave amplitude and zonal wind over the entire coherent range, except at the lowest frequencies, where they are 1/8 to 1/4 cycle out of phase. The phase spectrum in Fig. 1(d) shows 100 mb heat flux leading 10 mb wave amplitude (as expected for upward vertically propagating waves) by 1/8 to 1/4 cycle, except for the lowest frequencies, where they are in phase.

The relative coherency maxima and distinct phase relationships in Figs. 1(c,d) suggest two important time scales for planetary waves in the SH stratosphere: (1) transient waves with a time scale in the broad range of 5–30 days; and (2) quasi-stationary, seasonally-varying features with time scales greater than 30 days. The intention here is to study the stationary (low-frequency) and transient waves separately, and in relationship to each other and the zonal mean flow, by the use of simple time and zonal wavenumber filtering. The seasonally-varying (low-frequency) components are isolated by application of (approximately) 30-day running means; the half-amplitude response of such a filter is near 55 days. This simple technique is used (as opposed to more sophisticated digital filters) so that results are directly comparable with monthly mean statistics.

3. Seasonality

(*a*) *Zonal means*

Latitude–time plots of the low-frequency zonal mean zonal wind in the troposphere and stratosphere are shown in Fig. 2. NH data are included in the latitude–time plots here for comparison, although the primary discussions focus on the SH. In these and the following latitude–time plots three-day non-overlapping means were used to save computing space; low frequency is defined for these calculations as running averages of eleven adjacent three-day means, or 33-day running means. Although aspects of the zonal mean climatology in the SH stratosphere have been discussed by Labitzke and van Loon (1972), Knittle (1976), Hartmann (1976), Hirota *et al.* (1983), Mechoso *et al.* (1985), Barnett and Corney (1985), Farrara and Mechoso (1986), Newman (1986), Shiotani and Gille (1987), Geller and Wu (1987), among others, the zonal mean evolution is discussed here as a setting for the study of planetary wave variability. The 300 mb winds are included in Fig. 2 to illustrate seasonality in the troposphere, while 10 mb winds are representative of stratospheric variations.

Important aspects of the zonal flow seasonal evolution are:

(1) There is significant asymmetry between NH and SH, particularly in the stratosphere, where the SH mid-winter pole is colder and the polar night jet is nearly twice as

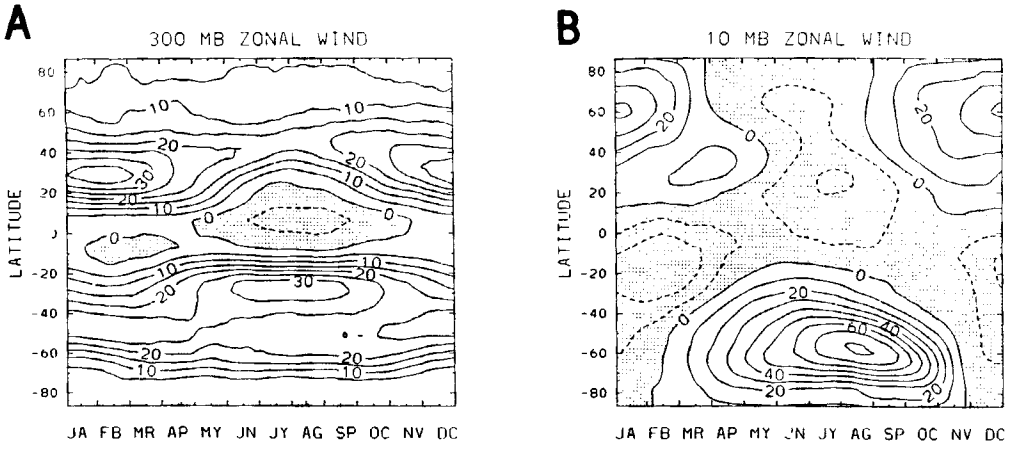

Figure 2. Latitude–time sections of the low-frequency zonal mean zonal wind at 300 and 10 mb (a,b). Units are $m\,s^{-1}$.

intense as in the NH. Note the separate low-latitude (~30°N) westerly maximum in the NH in March–April (Fig. 2(b)) that develops near the time of the breakdown of the high-latitude polar night jet—this is the lower limb of the subtropical mesospheric jet; a similar feature is not observed in the SH.

(2) Westerlies are established throughout the SH stratosphere by March. The core of the polar night jet is in the upper stratosphere throughout March–August, with strongest values in June–July. The core of the polar night jet descends to the middle stratosphere in September–October, as the spring transition to easterlies occurs first in the upper stratosphere. There is substantial interannual variability in the timing of the final warming, depending on the amount of planetary wave forcing (Farrara and Mechoso 1986; Newman 1986).

(3) A clearly defined winter configuration is found in the SH troposphere over May–October, with the subtropical zonal wind maximum at 300 mb being relatively constant over June–September (Fig (2a)).

Figure 3 shows meridional cross-sections of monthly mean SH zonal winds for April, June, August and October, along with two dynamically-important derived quantities: quasi-geostrophic potential vorticity gradient $\bar{q}_y$:

$$\bar{q}_y = \frac{2\Omega}{a}\cos\phi - \frac{1}{a^2}\frac{\partial}{\partial\phi}\left[\frac{1}{\cos\phi}\frac{\partial}{\partial\phi}(\bar{u}\cos\phi)\right] - (2\Omega\sin\phi)^2 e^{z/H}\frac{\partial}{\partial z}\left(e^{-z/H}\frac{1}{N^2}\frac{\partial\bar{u}}{\partial z}\right) \quad (1)$$

and quasi-geostrophic refractive index $Q_{k,c}$:

$$Q_{k,c} = \left[\frac{\bar{q}_y}{(\bar{u}-c)} - \frac{k^2}{a^2\cos^2\phi} - \frac{(2\Omega\sin\phi)^2}{4H^2N^2}\right] \Big/ \sin^2\phi. \quad (2)$$

Notation is standard in Eqs. (1) and (2): ϕ is latitude, $z = H\ln(P/1000\,\text{mb})$ is the vertical coordinate, $\bar{u}$ the zonal mean wind, k is zonal wavenumber, and c is zonal phase speed.

The potential vorticity gradient is a fundamental quantity in Rossby wave dynamics and stability of the zonal mean flow (Andrews *et al.* 1987); note the substantial variations in $\bar{q}_y$ in Fig. 3, related to curvature of the zonal wind fields. The refractive index is used to diagnose the influence of the zonal mean flow on Rossby wave propagation in the meridional plane. Linear wave theory predicts that, away from forcing regions, wave activity will flow along ridges of $Q_{k,c}$, be inhibited where $Q_{k,c}$ is small or negative, and

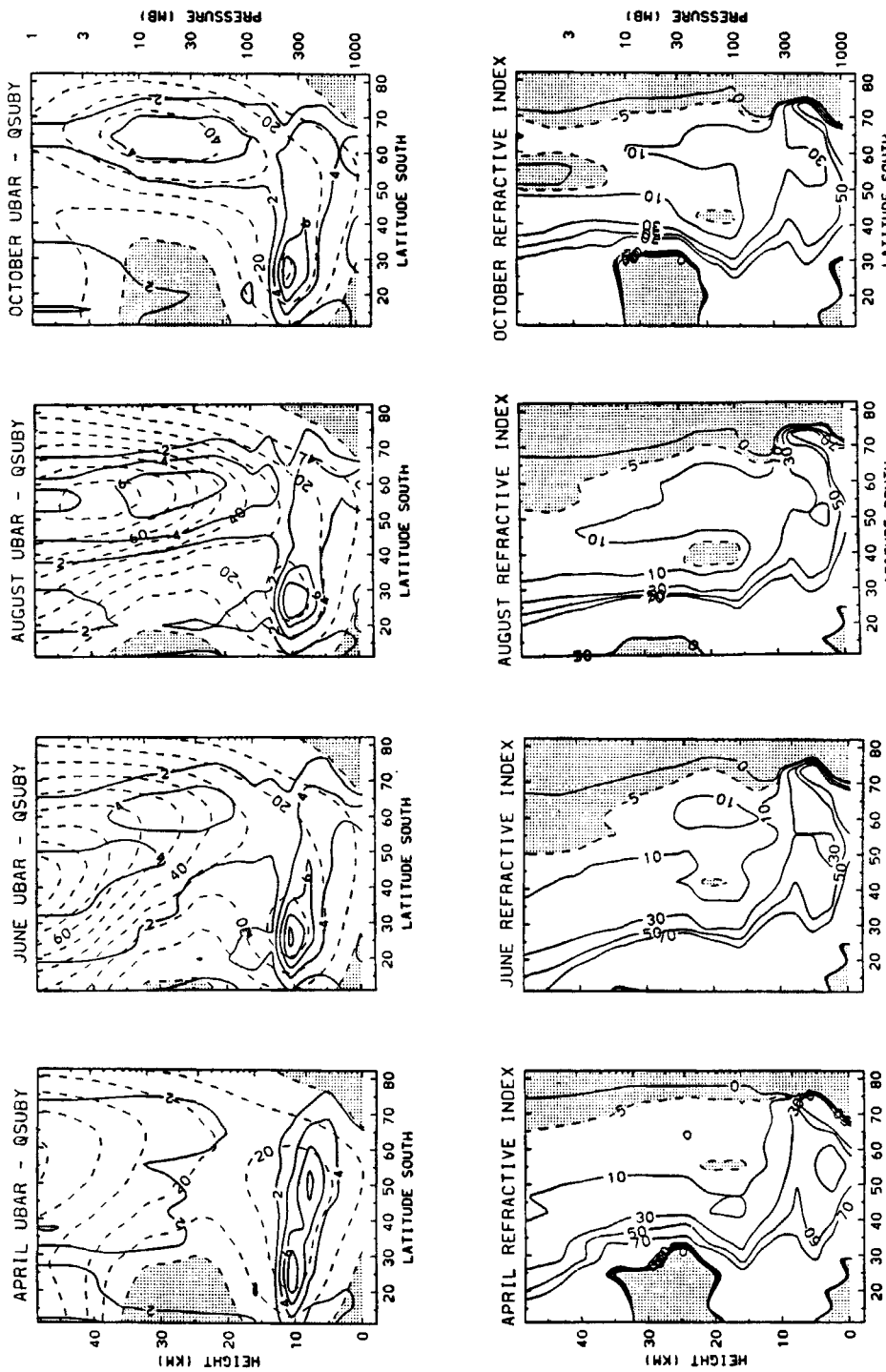

Figure 3. Top: Meridional cross-sections of the zonal wind (dashed lines, contours of 10 m s^{-1}) and quasi-geostrophic potential vorticity gradient (solid lines, contours of 10^{-11}m^{-1}s^{-1}); and bottom: quasi-geostrophic refractive index for stationary zonal wave 1 (Eq. (2)—units, 10^{-11}m^{-2}) for April, June, August and October. Refractive index values less than 5×10^{-11}m^{-2} in the lower figures are shaded, and values above 7×10^{-10}m^{-2} are not plotted.

be refracted toward larger $Q_{k,c}$ values (Palmer 1982; Smith 1983). Several studies have confirmed such behaviour in the NH stratosphere (Palmer 1981; O'Neill and Youngblut 1982; Smith 1983), although the wave–mean flow scale separation upon which linear theory is founded is certainly violated for planetary waves (the refractive index is usually a qualitative guide, and details should not be overemphasized). $Q_{k,c}$ contours in Fig. 3 are calculated for stationary zonal wave 1 ($k = 1$, $c = 0$), and the overall character is similar for other planetary waves whose phase speed is small compared with the zonal flow (during fall and spring, when the polar night jet is relatively weak, refractive index values for eastward-moving waves can be substantially different from those in Fig. 3—this aspect is discussed further in section 3(*d*)(iii). Intensity and position changes in the polar night jet over April–October are echoed in similar $\bar{q}_y$ variations in Fig. 3, with the result that the overall $Q_{k,c}$ structure remains fairly constant. June, August and October all exhibit a ridge of relatively high $Q_{k,c}$ in the high-latitude lower stratosphere, suggesting this to be the preferred location for vertical wave propagation from the troposphere into the stratosphere. August shows the largest such region of high $Q_{k,c}$, suggesting vertical wave propagation to be somewhat more viable during this time.

Figure 4(a) shows a measure of the transient fluctuations in zonal mean temperature at 50 mb, here defined as

$$T' = \left(\frac{1}{8}\sum_{i=1}^{8}(T_i - \bar{T}_i)^2\right)^{1/2} \tag{3}$$

where T_i is the three-day non-overlapping mean zonal temperature and $\bar{T}_i$ is the low-frequency temperature value for year i. Because relatively little power is contained in high-frequency (<5 day) motions in the stratosphere (cf. Figs. 1(a,b)), the transient variability is accurately represented by the three-day means used here (the spectral response of the effective time filter in Eq. (3) is near 5–50 days). Eleven-point running means of T' are displayed in Fig. 4(a) to highlight the seasonality. Distinct peaks in temperature fluctuations are found at the SH pole in May–June and October–November. Figure 4(b) shows the zonal wind transience at 10 mb, and two peaks in variance in high southern latitudes are observed during these same times—these are the thermal wind responses to the temperature variations in Fig. 4(a). The SH spring fluctuations are approximately twice as large as those of early winter. The NH variations in Fig. 4 are substantially larger than those in the SH, and are strongest in mid-winter (December–March).

(*b*) *Wave statistics*

Figures 4(c,d) show latitude–time sections of two measures of planetary wave activity in the stratosphere: 10 mb geopotential height variance and 100 mb poleward eddy heat flux (which is proportional to the vertical component of Rossby wave activity flux from the troposphere—see, e.g., Andrews *et al.* 1987). Root mean square wave amplitudes in Fig. 4(c) are calculated from

$$|Z_{\text{rms}}| = \left(\frac{1}{8}\sum_{i=1}^{8}\sum_{k=1}^{3}(ZS_{i,k}^2 + ZC_{i,k}^2)\right)^{1/2} \tag{4}$$

where $ZS_{i,k}$ ($ZC_{i,k}$) is the three-day non-overlapping mean value of the zonal wavenumber k sine (cosine) coefficient for year i. Both Figs. 4(c,d) show two maxima in the SH, in May–June and September–November; these are timed similarly to the zonal temperature and wind fluctuations in Figs. (4a,b). The later (spring) wave maxima are substantially larger than those of May–June. Stratospheric poleward momentum flux seasonality (not

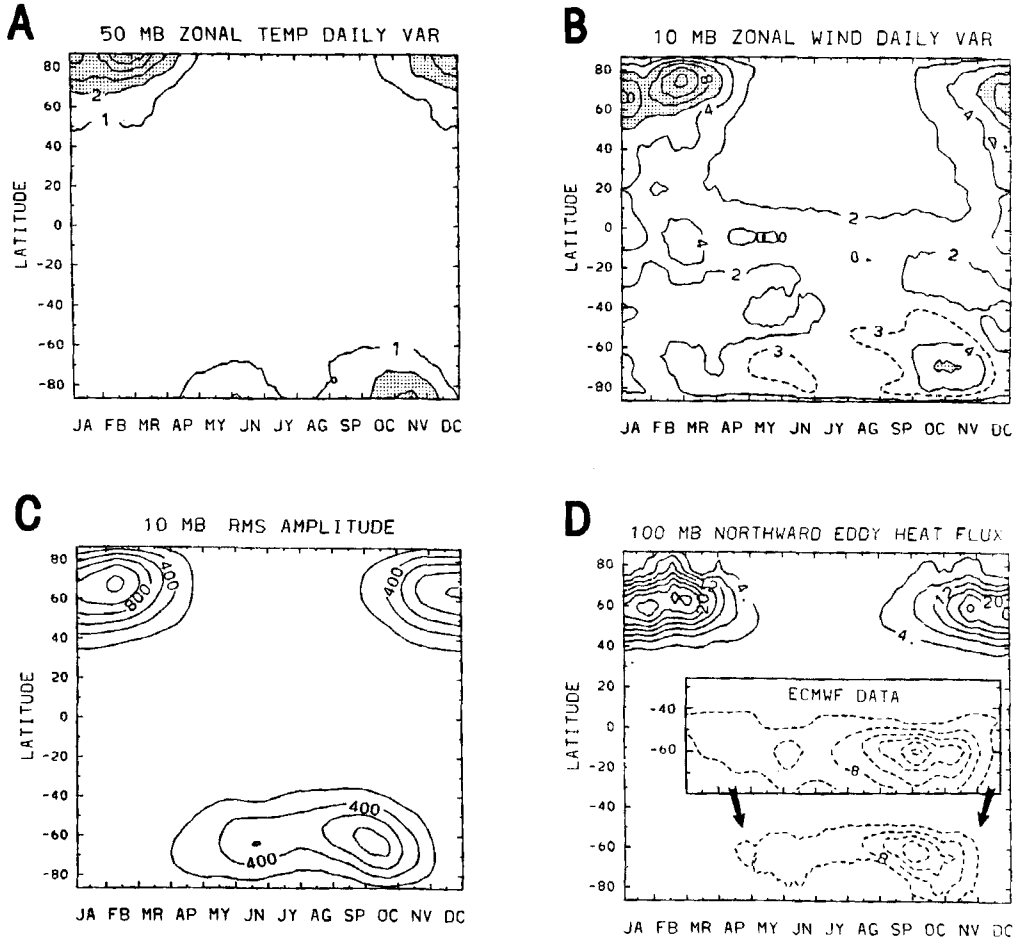

Figure 4. Latitude–time sections of (a) zonal mean temperature transience (Eq. (3)) at 50 mb (units, K); (b) zonal mean wind transience at 10 mb (units, $m\,s^{-1}$); (c) r.m.s. wave amplitude (Eq. (4)) at 10 mb (units of m); and (d) 100 mb northward eddy heat flux (units, $K\,m\,s^{-1}$). The inset in (d) shows estimates of SH heat flux from ECMWF data.

shown) is very similar to that of the heat flux in Fig. 4(d). The NH wave signatures show larger values (as do the zonal mean fluctuations), with a single maximum over November–March.

It is worth noting that the 100 mb SH NMC-derived heat fluxes in Fig. 4(d) are biased low by approximately 2–6 $K\,m\,s^{-1}$ compared with those analysed by the European Centre for Medium Range Weather Forecasts (ECMWF); ECMWF data for the SH are included in Fig. 4(d) for comparison. ECMWF 100 mb heat flux estimates in the NH (not shown) are in good agreement with NMC data in Fig. 4(d). The differing estimates in the SH are also shown in the comparisons done by Trenberth and Olson (1988b) and Newman and Randel (1988); the latter also demonstrate that it is the differing analyses of *transient* fluxes which account for this discrepancy. In spite of this bias, the ECMWF analysed values show two clear maxima (near 8 $K\,m\,s^{-1}$ and 24 $K\,m\,s^{-1}$, respectively), timed identically to the NMC maxima in Fig. 4(d).

Figure 5 shows latitude–time sections of geopotential fluctuations divided into stationary and r.m.s. transient zonal wave-1 and -2 components. Stationary wave ampli-

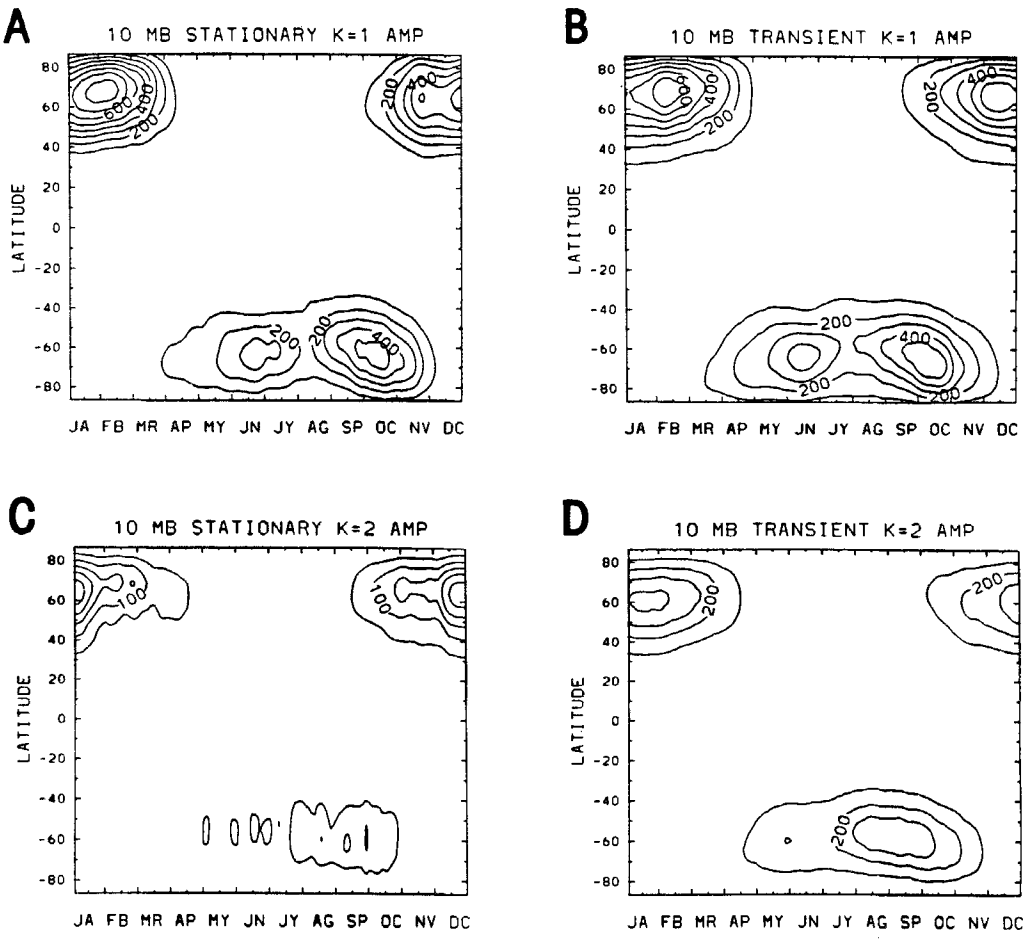

Figure 5. Latitude–time sections at 10 mb of the stationary (Eq. (5)) and r.m.s. transient (Eq. (6)) waves 1 and 2 individually. Units, m.

tudes for zonal wavenumber k are calculated from

$$|Z_{st}|_k = (\overline{ZS}_k^2 + \overline{ZC}_k^2)^{1/2} \tag{5}$$

where the overbar denotes an eight-year average of the 33-day running mean (low frequency) values. Root mean square transient wave amplitudes for zonal wavenumber k are given by

$$|Z_{tr}|_k = \left(\frac{1}{8}\sum_{i=1}^{8} (ZS_{i,k} - \overline{ZS}_k)^2 + (ZC_{i,k} - \overline{ZC}_k)^2\right)^{1/2} \tag{6}$$

with definitions as above. Transients here thus refer to both zonally-propagating features, and those which do not move but whose amplitude fluctuates in time. Wave fluxes are calculated in a similar manner, with stationary components calculated from the eight-year average Fourier coefficients. Only zonal waves 1 and 2 are shown here because they dominate the variance in the stratospheric wave fields. The r.m.s. total and transient values are smoothed with 11-point running means to emphasize seasonal variations.

The 10 mb geopotential variance maps in Fig. 5 show two pronounced maxima in the SH for the stationary wave-1 and transient wave-1 contributions (this behaviour for stationary wave 1 was noted by Hirota *et al.* 1983). The first maximum at 10 mb occurs in June and the second in October; similar patterns are observed at 1 mb (not shown), with the two maxima occurring approximately one month earlier there (April–May and September, respectively). The SH stratospheric variance is nearly equally partitioned between stationary and transient wave-1 features, with transient wave 2 also contributing in middle-to-late winter (note there is a small but distinct secondary maximum for transient wave 2 in early winter also). Transient wave 3 (not shown) has a seasonal signature similar to that of transient wave 2 in Fig. 5(d), with maximum values near 100 m; stationary waves 2 and 3 contribute negligible variance in the SH stratosphere. The NH patterns in Fig. 5 show substantially larger variance maxima than in the SH, with the distribution among various components similar to that in the SH (except for stationary wave 2).

In order to illustrate seasonality at other pressure levels, Fig. 6 shows height–time sections at 60°S of the (a) low-frequency zonal wind and (b) zonal wind transience, along with (c) the amplitude of stationary wave 1, and (d) transient wave 1; here the wave amplitudes are scaled with the square root of pressure to remove the effect of density stratification. (The use of three-day non-overlapping means in the troposphere removes a small percentage of the transient wave variance, although the patterns in Fig. 6 are virtually unchanged using daily data.) The zonal wind evolution in Fig. 6(a) illustrates the strongest mid-winter values, and shows that the spring transition (September–November) is much more rapid than that of fall (March–May). The largest zonal wind transience at 60°S (Fig. 6(b)) is observed during October in the middle-to-upper stratosphere, with a much smaller early winter maximum. The wave maxima in

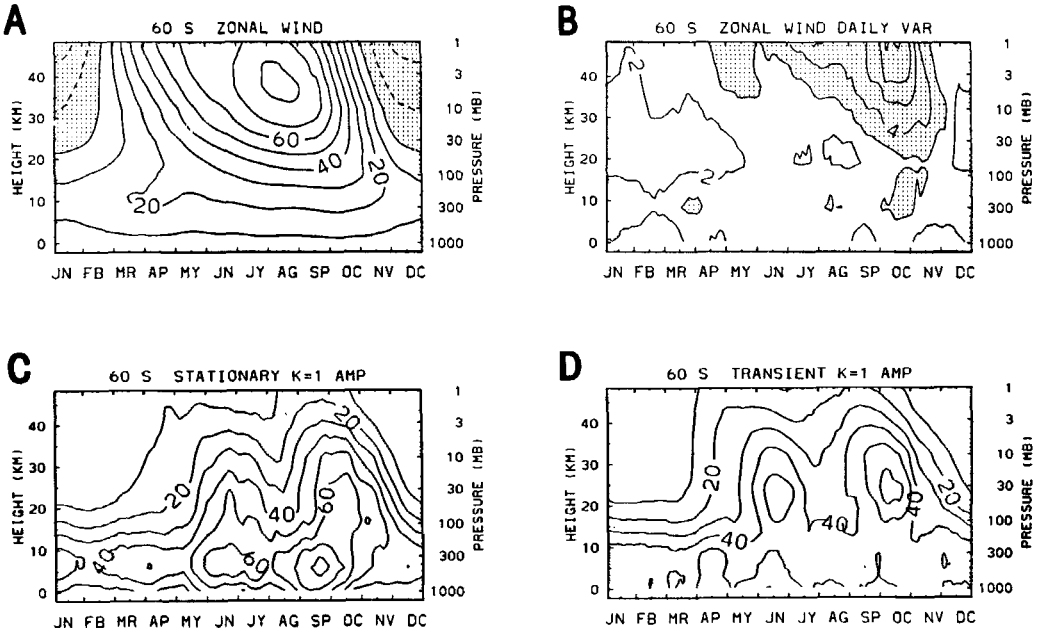

Figure 6. Height–time sections at 60°S of: (a) low-frequency zonal wind, and (b) zonal wind transience (Eq. (3)); along with amplitudes of stationary wave 1 (c); and transient wave 1 (d). Wave amplitudes in (c,d) are scaled with the square root of pressure. Units are m s^{-1} in (a,b), m in (c,d).

Figs. 6(c,d) occur earliest in the upper stratosphere, with maxima occurring later at lower levels down to 100 mb (this is also true for the mid-winter minimum). The transient and stationary wave-1 patterns reveal quite distinctive vertical structures; this behaviour will be discussed in more detail in following sections. Note the stationary wave-1 patterns show a double maximum (in time) even in the middle-to-upper troposphere (Fig. 6(c)).

Figure 7 shows geopotential variance latitude–time sections at 300 mb. The total planetary wave variance (Eq. (4)) in the SH upper troposphere (not shown) reveals a maximum during June–October over all mid-latitudes, timed similarly to the development of the winter subtropical tropospheric jet shown in Fig. 2(b). Stationary wave 1 (Fig. 7(a)) shows a maximum in low (30°–40°S) latitudes during June–October, and a maximum near 60°S all year. The high-latitude maximum near 60°S is modulated in time with a small maximum in June and a pronounced peak in August–October (this is more clearly seen in Fig. 6(c)). Transient planetary waves show less distinctive seasonality in the SH, with rather constant values over April–October. Although not accounting for much variance, stationary waves 2 and 3 in the SH also show clear seasonality: wave 2 (Fig. 7(c)) exhibits a clear but weak low-latitude (30°–40°S) maximum over June–September similar to that of stationary wave 1, while wave 3 (not shown) is strongest in mid-latitudes

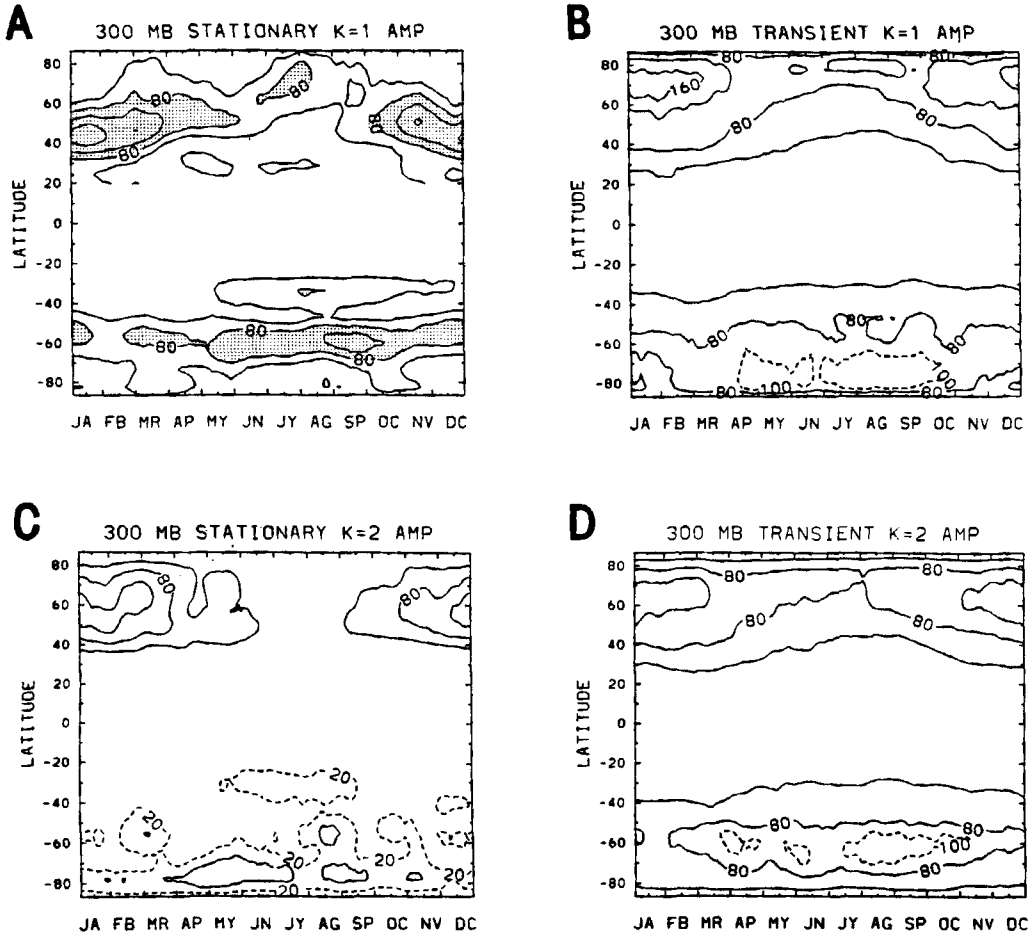

Figure 7. As Fig. 5, but for 300 mb.

(40°–60°S) over February–July. The NH variance patterns in Fig. 7 show larger values and stronger seasonality than in the SH, particularly for the transient components.

The seasonality in stationary waves at 300 mb (Fig. 7) is more pronounced, but similar overall to 500 mb patterns (not shown). Stationary planetary waves at 500 mb in the SH have been documented by van Loon and Jenne (1972), based on monthly mean maps of Taljaard *et al.* (1969) (which are representative of 1957–1966), Trenberth (1980), based on a six-year average (1972–1977) of monthly means from Australian analyses, and Karoly (1985), who used ten years (1973–1982) of daily Australian analyses. Additionally, the latter author has provided numerical values of the monthly means over 1000–100 mb for detailed comparisons (D. Karoly, 1987, personal communication). Comparisons with the present analyses are made in light of: (1) differences in the observing and analysis systems; and (2) different years of observations. In addition, these previous studies used interpolated monthly means, whereas the running means used here allow more detail in the seasonality to be analysed. In spite of these caveats, overall excellent agreement between these three data sets is observed (the July minimum in high-latitude stationary wave-1 amplitude in the upper troposphere is even apparent in the Australian data), promoting confidence in the accuracy of the tropospheric stationary waves in the present data.

(c) *SH stationary wave-1 evolution*

Examination of the structure of stationary wave 1 in the SH shows large changes between the early and late winter amplitude maxima; these changes are revealed in the EP flux cross-sections for stationary wave 1 during June and October shown in Figs. 8(a,b). Relatively small EP flux vectors are seen in June (Fig. 8(a)), resulting from small phase tilts in height and latitude (in particular, an equivalent barotropic vertical structure). In contrast, strong vertical EP flux (poleward eddy heat flux) is seen in high latitudes above 300 mb in October (Fig. 8(b)), along with much stronger wave driving throughout the stratosphere. In fact, the stationary wave-1 component completely dominates the maxima in poleward fluxes of heat and momentum during September–November (seen in Fig. 4(d)), and the transients assume a secondary role (the climatological contributions from stationary and transient waves are shown in Randel (1987c)). These seasonal changes in EP flux (Figs. 8(a,b)) are much more pronounced than those in wave amplitude (e.g., Fig. 6(c)), suggesting a fundamental change in the (vertical) structure of the wave. This is confirmed in Fig. 9, which shows the seasonality in phase of stationary wave 1 at 60°S at 700, 300, 50 and 10 mb; this illustrates the temporal development of the vertical phase structure. This figure was produced by low-pass filtering the individual Fourier components in an analogous manner to the stationary wave amplitude calculations (Eq. (5)). (Monthly mean wave 1 data at 300 mb from the Australian data set are also shown in Fig. 9 for comparison.) Comparison with the stationary wave-1 amplitude at 60°S (Fig. 6(c)) shows that the smallest vertical phase tilts (i.e., closest vertical spacing in Fig. 9) are observed during the June–July amplitude maximum. Subsequently, the tropospheric (700 and 300 mb levels) crest moves eastward, and the stratospheric (50 and 10 mb levels) crest moves rapidly westward, so that the September–October wave is strongly baroclinic (in addition to achieving maximum amplitude).

Both the June and October stationary wave-1 EP sections in Fig. 8 reveal a region of positive EP flux divergence near 60–70°S and 300 mb; under conservative conditions, such regions may suggest source regions for local wave activity (nonlinear wave forcing could be one cause of such a source region; note the EP flux divergence in this region from all waves is negative (Mechoso *et al.* 1985)). There is also a region of strong positive divergence in October in the middle stratosphere near 60–70°S; this pattern persists when

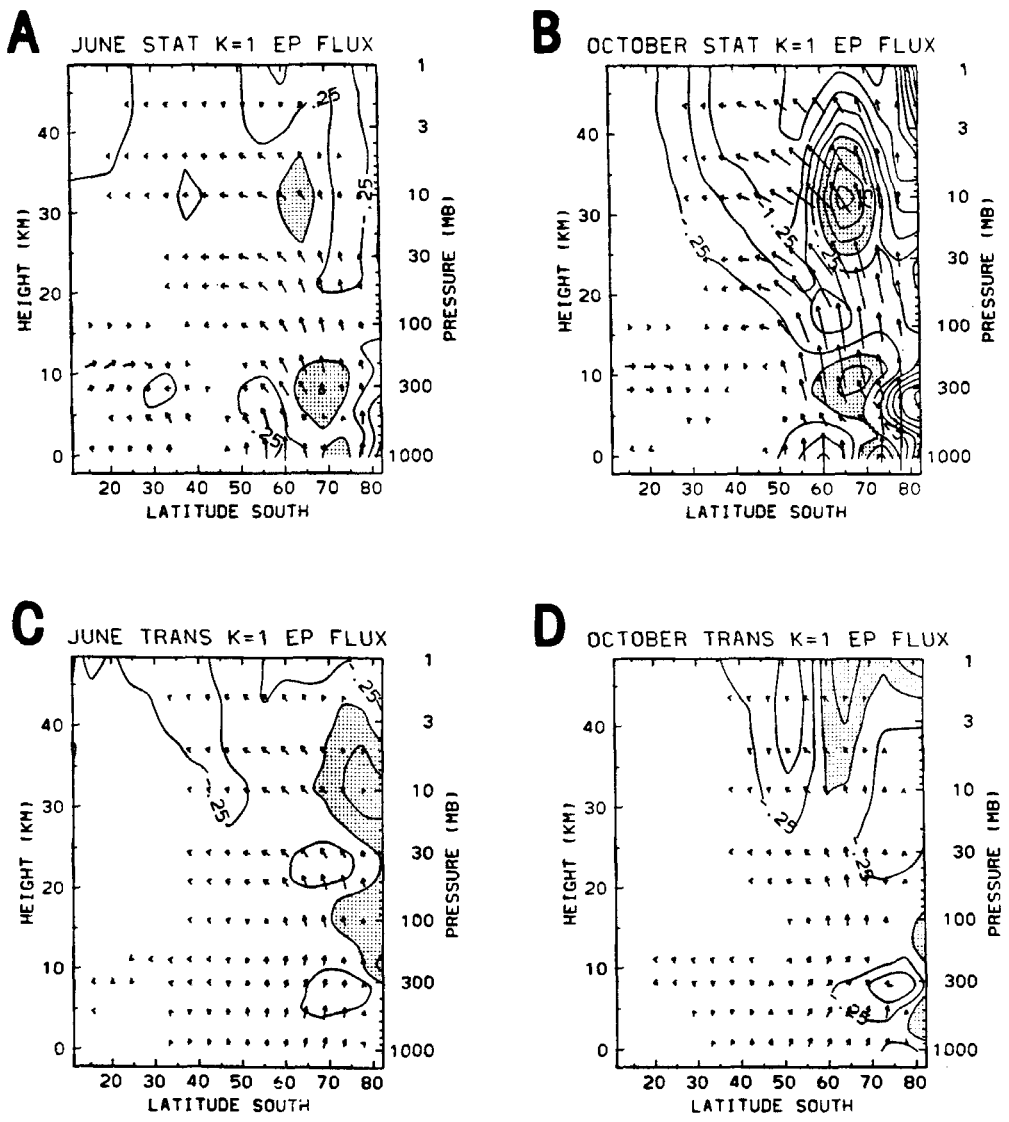

Figure 8. Monthly-averaged EP flux diagrams for stationary and transient wave 1 in June and October. Wave-driving contours of ±0·25, 0·75, . . . , with values greater than 0·25 shaded. The vector scaling is identical in (a) to (d).

all other waves are included. Because strong positive $\bar{q}_y$ in this region (Fig. 3) precludes internal instability, the nature of this feature is uncertain (see Andrews 1987 for discussions regarding interpreting such observed patterns).

The low-latitude upper tropospheric EP vectors in Figs. 8(a,b) also suggest wave activity propagation from low latitudes or the tropics; this signature is somewhat stronger in August (not shown), and prominent for stationary wave 2 (not shown). These observations suggest that the low-latitude (30–40°S) tropospheric amplitude maximum for stationary waves 1 and 2 (see Figs. 7(a and c)) may be related to tropical/subtropical forcing.

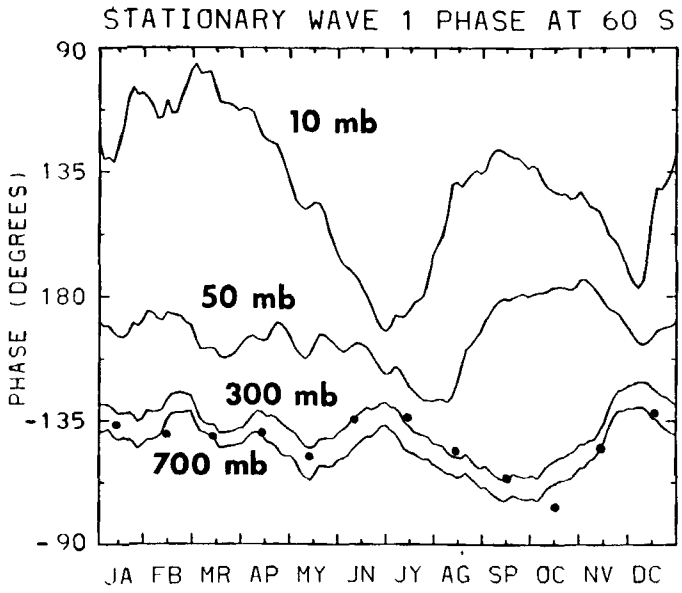

Figure 9. Seasonality in phase (longitude of crest) of stationary wave 1 at 60°S for various pressure levels; compare with stationary wave-1 amplitude in Fig. 6(c). The dots indicate monthly mean 300 mb data from Australian climatology. Note the small westward phase tilt with height in June–July versus large tilt in September–October.

(*d*) *Transient planetary wave seasonality*

(i) *Structure in the meridional plane.* Figures 5(c) and 6(d) reveal distinct early and late winter wave amplitude maxima for transient wave-1 geopotential fluctuations in the SH stratosphere, similar to the stationary wave-1 signature. However, in contrast to the pronounced structural changes for stationary wave 1 discussed above, transient wave 1 exhibits similar poleward heat flux and EP flux variations during early and late winter, as shown in their EP flux signatures in Figs. 8(c,d), suggesting similar character of the transients over both periods (and clear distinction from the stationary component). A second clear distinction between stationary and transient wave 1 is the vertical amplitude structure observed of each: figures 6(c,d) clearly show that the transients have a (density-weighted) amplitude maximum in the lower-middle stratosphere, while the stationary wave is largest in the middle-upper troposphere. An interesting comparison is with the numerical model results of Robinson (1986b), who shows enhanced stratospheric amplitudes for eastward-moving (versus stationary) wave 2, as a response to the same lower-level forcing (transient wave 1 here is also eastward moving). However, the mechanisms behind these observations await explanation.

The transient wave meridional structure in the SH stratosphere is similar to that of stationary wave 1 for each month (cf. Fig. 5), whereas markedly different patterns are observed in the troposphere. Because of the geometry of converging meridians at high latitudes, much of the geopotential variance is contained in low zonal wavenumbers; analysis of *coherent* zonal wave-1 fluctuations in the troposphere reveal three out-of-phase meridional maxima that are quite distinct from the monotonic latitudinal increase seen in time-averaged statistics (Randel 1987a). The three-cell tropospheric structure for wave 1 discussed in Randel (1987a) is most pronounced during June and (particularly) August, during the well defined winter period when stationary wave 1 at low latitudes

(30–40°S) is strongest. Furthermore, the three tropospheric meridional coherence maxima for transient wave 1 are centred near 20°, 45° and 70°S, coincident with the minima in stationary wave 1 (Fig. 7(b)), showing a degree of meridional orthogonality between stationary and transient wave-1 variance in the troposphere.

(ii) *Zonal propagation.* Zonal propagation is studied via time–longitude lag correlation diagrams, as recently introduced by Fraedrich and Lutz (1987), which allow statistical measures of zonal wavelengths, phase and group velocities. To study seasonality, correlation statistics are calculated from 60-day time series centred on April, June, August and October; only the June and October results are shown here (to contrast behaviour during the two maxima in transient wave variance). Overall, statistics are similar during April–June and August–October. Stationary waves (defined as the sixty-day mean) are removed for each year, and the statistics are averaged appropriately over the eight years of data. Significance levels for the correlations are estimated as in Fraedrich and Lutz, with the result that correlations greater than approximately 0·05 are significant at the 5% level. Figure 10 shows such diagrams calculated from zonal waves 1–12 at 10 mb and 56°S, for June and October. The dominant scale of zonal fluctuations is given by twice the distance between maximum and minimum of the simultaneous correlations. A predominant zonal wavenumber-1 signature is found in June (in agreement with the variance patterns of Fig. 5), whereas significant contributions from zonal wave 2 in October result in a statistical wavelength of about 210° longitude.

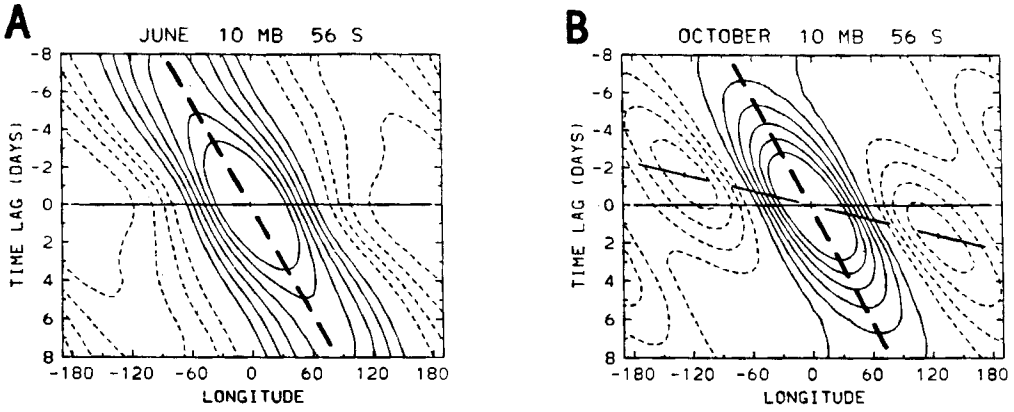

Figure 10. Time–longitude lag-correlation diagrams at 10 mb and 56°S for June and October. Contours of ±0·1, 0·2, . . . , 0·6; see text for significance levels. Heavy dashed lines indicate eastward phase speeds (near 7 m s ^{1}), while lighter dashed lines in October denote eastward group velocity (near 65 m s^{-1}).

The zonal phase velocity is indicated by the slope in time of the maximum positive or negative correlation coefficients, as denoted by heavy dashed lines in Fig. 10. There is a lack of seasonality in zonal phase velocity in Fig. 10, with both months exhibiting eastward phase velocity near 10–15 m s^{-1}. This lack of seasonality is surprising in light of the large seasonal intensity variations of the polar night jet (cf. Fig. 3), but may be explained to some degree by noting that there are large corresponding variations in the zonal mean potential vorticity gradient (Fig. 3). These two factors act to cancel one another in the Rossby dispersion relation, so that large zonal wind variations may not be directly reflected in zonal phase velocity changes.

Diagrams such as in Fig. 10 can be constructed for each zonal wavenumber separately to estimate zonal phase speeds. Table 1 displays the resulting estimates for waves 1 to 3

TABLE 1. ESTIMATED ZONAL PHASE VELOCITIES

	April	June	August	October
1 mb				
$k = 1$	7	8	13	9
$k = 2$	5	4	8	6
10 mb				
$k = 1$	7	8	4	5
$k = 2$	5	9	7	10
$k = 3$	5	8	9	12
300 mb				
$k = 1$	−1	−3	0	−1
$k = 2$	1	1	2	2
$k = 3$	4	4	5	5

In $m\,s^{-1}$, positive eastwards.

separately at 60°S for 1, 10 and 300 mb. All the waves are eastward moving throughout the stratosphere during April–October; only wave 1 at 300 mb is quasi-stationary or slightly retrogressive. Increased eastward zonal phase speed is observed for the shorter waves during all months at 300 mb, and at 10 mb during August–October, when waves 2 and 3 contribute significant fractions of the variance (cf. Fig. 5). During April and June at 10 mb, and all months at 1 mb, wave 1 moves fastest toward the east (note, however, that there is insignificant power beyond wave 1 during these times).

Zonal group velocities can be determined from the time–longitude lag-correlation diagrams by the slope of the line which connects the correlation maximum in the centre with the neighbouring minima at positive and negative time lags (see Fraedrich and Lutz 1987). This slope is clearly defined at 10 mb for October and indicated in Fig. 10, suggesting an eastward zonal group velocity near $65\,m\,s^{-1}$. Note that because a single zonal wavenumber (wave 1) dominates the stratospheric variance in June, no zonal group velocity is observed (a single wave cannot form a wave packet or disperse).

(iii) *Vertical and meridional propagation.* Vertical and meridional propagation of transient planetary waves is studied via modified longitude–time lag-correlation diagrams, introduced in Randel (1988), which allow tracing of coherent fluctuations in the zonal–height or zonal–meridional planes. Groups of such diagrams clearly show vertically or meridionally-propagating Rossby wave trains; calculation details, examples for NH and SH data, and associated discussions are found in Randel (1988). Figure 11 shows such longitude–height diagrams at 56°S for June and October, for time lags of 0, +2 and +4 days, using a reference position at 300 mb (denoted as an × in the lag-0 plots). These correlation maps show eastward- and vertically-propagating wave trains, with clear propagation of planetary waves into the stratosphere downstream of the wave source. Very similar eastward and vertically propagating wave packets were shown by Marks (1988) in his analyses of stratospheric model results. Note that the diagrams in Fig. 11 are the zonal average of 36 such correlation maps calculated every 10° in longitude (the longitude scale thus denotes *relative* separation, not geographic longitude)—averages over restricted longitudes have shown that there is not a strong dependence on longitude reference position for any of the patterns in Fig. 11.

An interesting feature in Fig. 11 is the strong positive stratospheric correlations approximately 180° downstream in October, which are weak or absent in June. The reason for this is that the June wave trains are refracted strongly equatorward, and thus

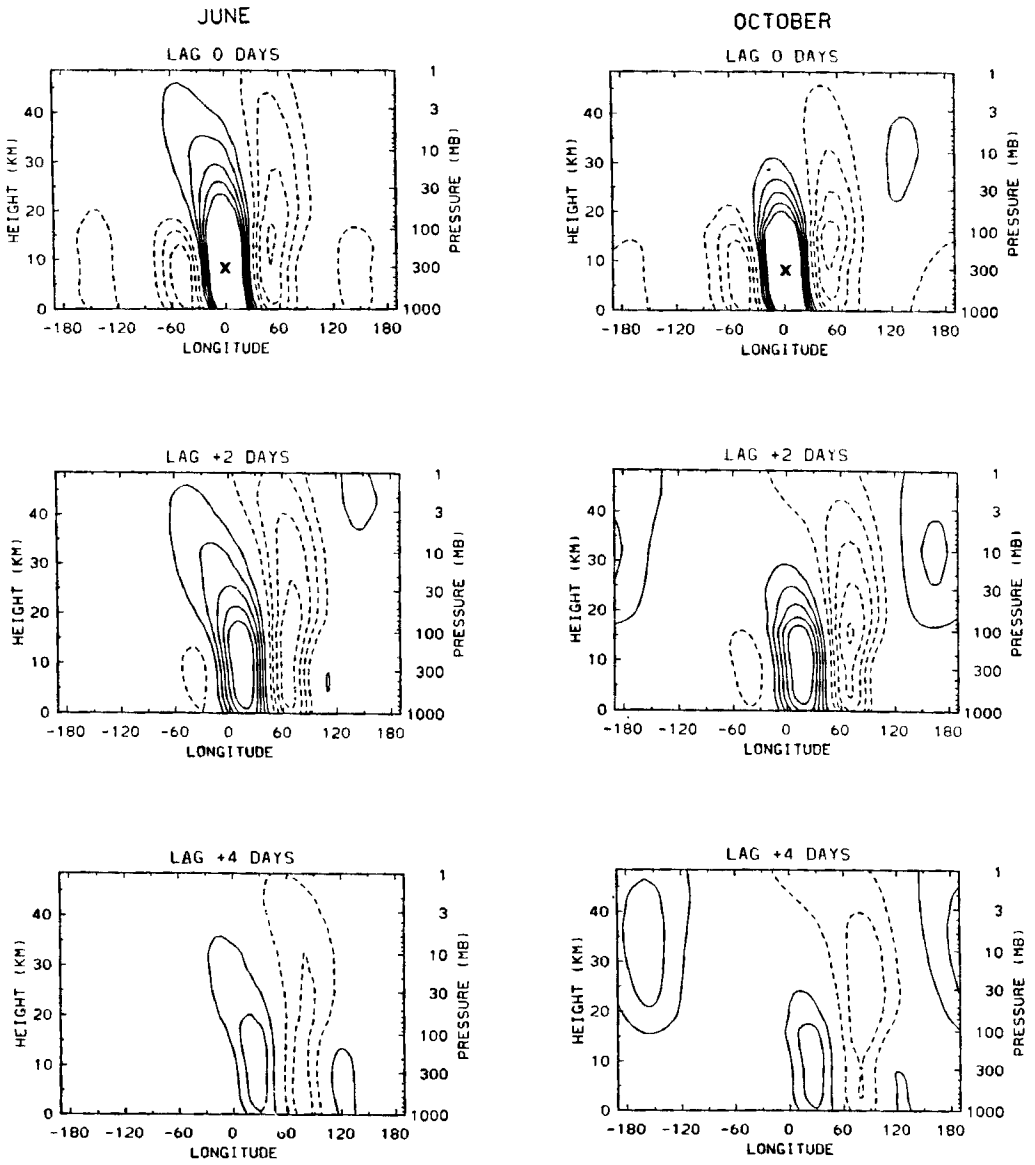

Figure 11. Longitude–height sections of geopotential correlations with respect to 300 mb, for time lags of 0 (top), +2 (middle), and +4 (bottom) days, for June and October. Contours of ±0·075, 0·150, . . . , . Longitude reference scale denotes relative displacement, not geographic longitude. Note eastward- and vertically-propagating wave trains, and propagation of planetary scales into the stratosphere.

not visible downstream at the same latitude. To illustrate this, Fig. 12 shows latitude–longitude diagrams of the 10 mb correlations with respect to 300 mb, 56°S at a time lag of three days, i.e., these show the meridional–zonal structure of the stratospheric wave trains which are coherent within the troposphere. Again, these are zonally-averaged diagrams, and the longitude scale denotes relative distance from the 0° (six o'clock) reference position (which is at 300 mb). Figure 12 shows that the early winter wave trains propagate with a strong equatorward component, with strongest positive correlations some 20° equatorward (and 110° downstream) of the 56°S reference position. The October

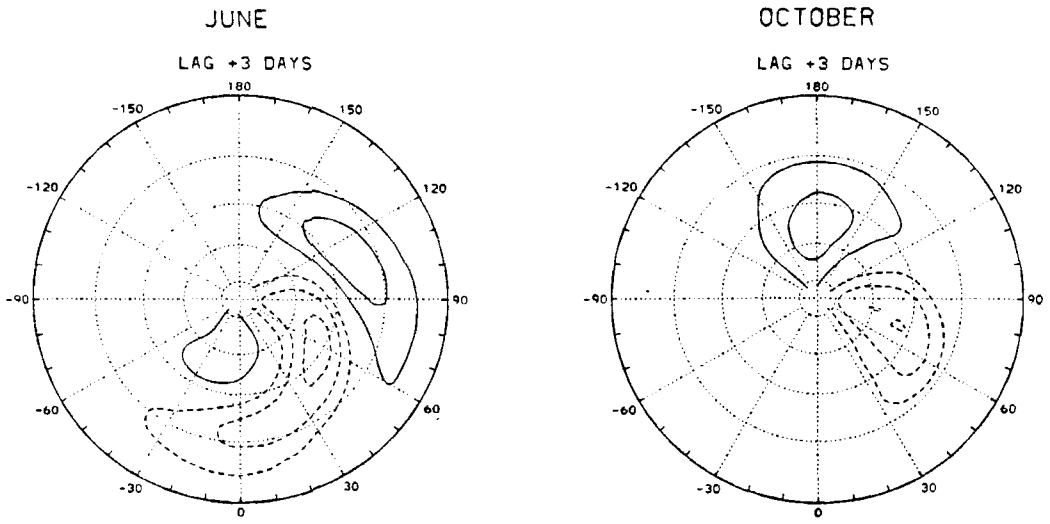

Figure 12. Latitude–longitude diagrams of the geopotential correlations at 10 mb, for a time lag of +3 days, with respect to a reference position at 300 mb and 56°S. These show the meridional structure of the stratospheric wave trains in the lower panels of Fig. 11. Latitude spacing is 20°, with the outermost latitude the equator. Longitude scale denotes relative distance from the zero degree (six o'clock) 300 mb reference position. Note that these SH grids have been reversed, so that eastward is counterclockwise. Contours as in Fig. 11.

patterns in Fig. 12 reveal primarily zonal propagation (August shows a situation midway between these extremes). The observed strong meridional refraction in June versus little in October is consistent with changes in the basic state propagation characteristics. Refractive index calculations (Eq. (2)) for June and October using zonal wavelength and phase speed information from Figs. 10(a,b) show little qualitative change for June (when the zonal winds are much stronger than the observed $7\,m\,s^{-1}$ wave phase speed), but substantial differences in October. In particular, weak zonal winds on the equatorward flank of the polar night jet (near 45°S) in October result in a critical layer in this region (i.e., $\bar{u} = c$), and a change in sign of $Q_{k,c}$. Positive values of $Q_{k,c}$ are then observed only over approximately 45–75°S in the middle stratosphere, suggesting a type of cavity in this region for wave propagation (and a restriction of equatorward propagation). Note the transient wave EP flux vectors in June show stronger meridional components than those in October (compare the 50 and 30 mb vectors in Figs. 8(c,d)), consistent with the correlation statistics (Fig. 12) and mean flow changes discussed above. A future paper will quantify such observations and compare with linear Rossby wave theory.

(iv) *Dynamic life cycles.* One method to analyse the evolving dynamical signatures of the vertically-propagating planetary waves is via lag correlations between stratospheric wave variance and EP flux diagnostics at each latitude and height. Figure 13 shows groups of EP flux correlation diagrams calculated as follows: the vertical vector component at each position measures the correlation between 10 mb geopotential variance and the vertical EP flux vector component at that latitude and height, while the horizontal vector component measures a similar correlation with the horizontal EP flux vector component. Furthermore, contours are added of the correlations between geopotential variance and EP flux divergence. For these calculations the geopotential variance at 10 mb is averaged over 40–70°S (to represent a broad measure of stratospheric wave activity), and only zonal waves 1 and 2 are used to construct the various wave quantities (inclusion of higher

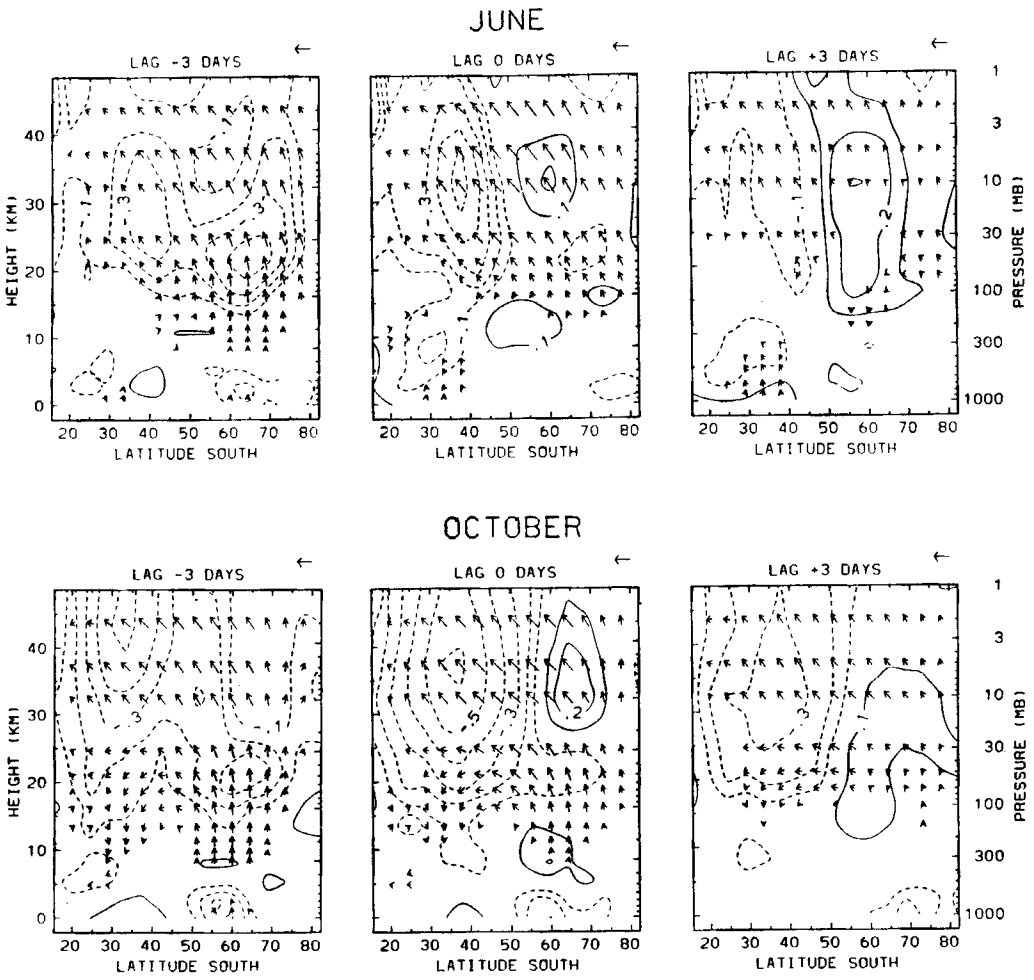

Figure 13. Meridional cross-sections showing the correlation between 10 mb geopotential variance and components of the EP flux vector and its divergence at each latitude and height for zonal waves 1 and 2. Each vector is drawn such that the vertical component measures the correlation with the vertical component of the EP flux vector at that position, and similarly for the horizontal components. The reference arrows in the upper right-hand corners represent a component correlation of 1·0. Contours represent correlations with the EP flux divergence with values of ±0·1, 0·2, ... Diagrams are shown for time lags of −3, 0, and +3 days (with respect to the 10 mb geopotential variance time series), for June and October. Vectors are plotted only where the correlations are significant above the 90% confidence level (determined as described in appendix A of Randel (1987a)).

zonal wavenumbers reduces the observed correlations in the troposphere due to the inclusion of high-frequency fluctuations not related to planetary wave variability). The evolving patterns in Fig. 13 reveal EP flux variations which are coherent with the stratospheric wave amplitude fluctuations; it is important to remember, however, that these vectors and contours represent only *correlations*, and thus give no information as to the strength of the actual EP flux diagnostics at each position.

The overall patterns in Fig. 13 are similar for June and October, showing geopotential maxima in the stratosphere correlated with upward- and equatorward-pointing EP vectors (as seen in climatological time averages, i.e. Mechoso *et al.* (1985), and Fig. 8). The evolution in Fig. 13 shows strong correlations with vertical EP flux in the lower strato-

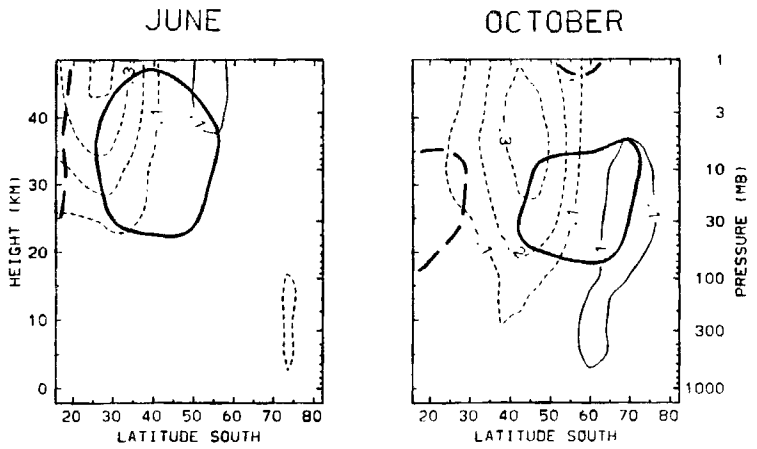

Figure 14. Meridional cross-sections showing the contemporaneous correlation between 10 mb geopotential variance and observed $\partial\bar{u}/\partial t$ (light lines) and $\partial\bar{T}/\partial t$ (heavy lines) for June and October. Contours for $\partial\bar{u}/\partial t$ correlations are $\pm 0{\cdot}1$, $0{\cdot}2$, . . . , while for clarity only the $-0{\cdot}1$ and $+0{\cdot}2$ $\partial\bar{T}/\partial t$ contours are shown. Positive correlations denote accelerations and warmings, respectively.

sphere over 50–70°S, prior to stratospheric wave variance maxima (lag −3 days); the correlations in this region drop abruptly below 300 mb, although there are still some significant upward vectors in the lower troposphere, particularly in October. The stratospheric patterns in Fig. 13 show strong correlations throughout the entire stratosphere (strongest near lag 0 days), with the maximum correlation regions moving somewhat equatorward from time lags of −3 to +3 days.

Evolution of the EP flux divergence correlations in Fig. 14 shows strong initial negative correlations in the high-latitude lower stratosphere (lag −3 days), followed by weakening of the negative patterns there (lag 0 days), and subsequent positive values (lag +3 days). Qualitatively very similar signatures are observed of tropospheric baroclinic wave life cycles (Edmon *et al.* 1980). Strong negative correlations are observed in the low-latitude stratosphere (largest near lag 0 days), while positive correlations are seen in the high-latitude stratosphere at lags 0 and +3 days; these correlations show clear transient wave modulation of the north–south stratospheric dipole pattern apparent in time average statistics (Mechoso *et al.* 1985).

The overall patterns in Fig. 13 are consistent with signatures expected of vertically-propagating waves originating in the troposphere—similar EP flux vector correlations are discussed in Randel *et al.* (1987), along with a compositing analysis suggesting a source region of transient planetary wave activity in the upper troposphere (possibly due to nonlinear interactions). Such a source region is also apparent in Fig. 14 as the positive correlation area in the high-latitude upper-troposphere near lag 0 days. Note also the negative correlations in high latitudes near the surface, suggesting that low-level baroclinic effects may also be important (i.e., cooperative behaviour between direct baroclinic wave growth and upper-level wave–wave forcing).

Only relatively minor differences are seen in Fig. 14 between June and October statistics. The similar correlation signatures in Fig. 13 are surprising in light of the distinctive meridional propagation characteristics suggested in Fig. 12; the statistical correlations in Fig. 13 suggest coherent wave variations in October well beyond the above mentioned critical line (near 40°S), although there is a hint in Fig. 13 of refraction away from the strongest low-latitude easterlies over 30–10 mb (Fig. 3).

Alternatively, quite striking June–October differences are observed for induced mean flow changes. Figure 14 shows contemporaneous correlation maps between 10 mb geopotential variance and (1) observed zonal wind acceleration ($\partial \bar{u}/\partial t$) and (2) observed zonal temperature tendency ($\partial \bar{T}/\partial t$); there are qualitatively minor changes in these patterns with time lag. Both months exhibit clear north–south dipole patterns of $\partial \bar{u}/\partial t$ (with stronger deceleration correlations equatorward); these sandwich the strongest warming patterns, with weaker patterns of cooling in low latitudes (note the thermal wind balance, and the fact that the most coherent warming patterns are in mid-latitudes). (For clarity, only the $+0{\cdot}2\,\partial \bar{T}/\partial t$ contour is shown in Fig. 14; positive maxima are of order 0·3–0·4.) These signatures are in good agreement with those anticipated due to localized wave driving (Dunkerton *et al.* 1981). An important feature in Fig. 14 is the pronounced June–October pattern changes: the October patterns are somewhat lower and shifted ~15° poleward. This systematic poleward shift of the wave-induced mean flow accelerations is in good agreement with the observed restricted meridional propagation and basic state refractive characteristics in October (Fig. 12), and is consistent with meridional trapping or high-latitude focusing of transient wave activity in the SH spring. Such effects can contribute to the occasional large effects of transient waves in the SH spring (Yamazaki and Mechoso 1985; Farrara and Mechoso 1986; Newman 1986).

4. Summary and discussion

Seasonality in stationary and transient wave structure in the SH stratosphere has been documented, based on an eight-year climatology that has previously been unavailable; a summary of important points is given here.

(1) Two distinct maxima in stratospheric geopotential height variance are observed in the middle and upper stratosphere during early winter and late winter–spring; Hirota *et al.* (1983) appear to be the first to have noted such behaviour for stationary wave 1 in the SH. These maxima sandwich the strong mid-winter zonal winds, and the entire sequence occurs approximately one month earlier in the upper stratosphere. The second maximum in wave variance (during September–October) is substantially larger than the first. These variance maxima are partitioned primarily between stationary and transient zonal wave 1, with transient wave 2 also contributing significant variance in late winter–spring.

The maxima in wave variance during June and October (and minimum in August) at 100 and 10 mb are not in agreement with the observed variations in lower stratospheric refractive index, which would suggest the strongest vertical propagation to occur in August (Fig. 3). This suggests that the system is more complex than a remote wave-like response to constant forcing. The fundamental pattern of two wave-variance maxima sandwiching the strongest zonal winds (which was also observed to a much lesser degree by Smith (1983) for stationary wave 1 in the NH stratosphere) is in good agreement with the recent model results of Wakata and Uryu (1987), who attribute this behaviour to multiple equilibria of the coupled planetary wave–zonal mean system. The distinctive timing of wave-variance maxima in the middle versus upper stratosphere (for both stationary and transient components), in conjunction with the clear tropospheric origins of the waves, suggests that the amplitude of geopotential anomalies at each height is determined to a large degree by the properties of the basic state. The distinctive vertical structure of stationary versus transient wave-1 height fluctuations awaits definitive explanation.

The 4–5-month time difference between early and late winter wave variance maxima

will contribute a significant amount of variance to the semiannual oscillation (SAO). A recent analysis of global stratospheric temperature data (Gao *et al.* 1987) highlighted several features of the SAO in the high-latitude SH, namely: (1) a prior occurrence in the middle versus lower stratosphere by 1–2 months; and (2) a pronounced longitudinally localized amplitude maximum centred near 60°S, with a scale of zonal wave 1 and westward tilt with height. These aspects are all in good agreement with the stationary wave-1 structure and evolution detailed here. In addition, the two maxima in wave-induced polar warmings in the SH (see Fig. 4(a)) contribute a significant amount of variance on the SAO time scale, as proposed by Gao *et al.*

(2) Wave-induced poleward fluxes of heat and momentum in the SH stratosphere have a pronounced maximum in September–October, during which time they facilitate the winter-to-summer transition in the stratosphere. A much smaller secondary maximum in poleward fluxes is observed in May–June; note that the polar warming effect of these heat fluxes is contrary to the strong radiative cooling occurring during this time, i.e., the waves are 'fighting' the seasonal transition. The observed wave driving is thus consistent with rapid spring and slow fall transitions in the stratosphere (i.e. Fig. 6(a)).

(3) Intriguing structural changes occur in stationary wave 1: the early winter amplitude maximum is predominantly barotropic, whereas the late winter–spring maximum is strongly baroclinic in the stratosphere. The September–October maximum in heat and momentum fluxes predominantly result from stationary wave 1, and the transient waves assume a secondary role (note that this is a climatological statement; rapid breakdowns of the spring polar vortex can occur in spring, a result of transient wave forcing (Yamazaki and Mechoso 1985; Newman 1986; Farrara and Mechoso 1986)).

The cause of this strong change in stationary wave-1 structure is unclear. Because the zonal flow in the troposphere does not change substantially between early and late winter, it is not anticipated that forcing by topography would be involved—this is also discounted by the observation that the change in vertical structure occurs in the upper troposphere–lower stratosphere (see Fig. 9). Differential interaction with the tropospheric transients in early and late winter is also one possibility, although there is no obvious change in the transient statistics during southern winter that would point to such a mechanism. Other mechanisms, such as direct diabatic forcing or more subtle nonlinear interactions, may be needed to explain these observations.

A great deal of success has been found in modelling the stationary wave structure of the NH winter, based on linearized equations that include topography and observed heating (e.g. Chen and Trenberth 1988, and references therein). SH planetary wave seasonality similar in some respect to that observed here was found in the annual cycle simulations of Holton and Wehrbein (1980), using a single wave–mean flow interaction model. James (1988) has used a succession of linear and nonlinear barotropic models to study planetary wave forcing in SH winter climatological flow, finding that a good deal of the observed horizontal structure can be understood as a linear response to forcing by Antarctica. Similar work using baroclinic models incorporating seasonally-varying mean flows and forcings may be needed to understand the maintenance mechanisms for the planetary waves observed here. Note that the low-latitude tropospheric stationary wave-1 EP flux in winter (Figs. 8(a,b)), along with the similar low-latitude stationary wave-2 EP flux signature (not shown), clearly suggest that low-latitude or tropical forcings cannot be neglected.

(4) Transient planetary waves exhibit less distinctive seasonality than their stationary counterparts, although clear changes occur over April–October. Longitude–time lag-

correlation diagrams reveal little seasonality in observed eastward phase progression throughout the stratosphere, in spite of large changes in corresponding zonal mean flows. The presence of significant zonal wave-2 and -3 variance in the middle stratosphere during August–October is associated with clear eastward group velocity (near 65 $m\,s^{-1}$) not observed during April–June (when wave 1 alone is predominant). Modified longitude–time lag-correlation diagrams reveal wave trains which propagate eastward and vertically from the troposphere into the stratosphere during all winter months in the SH. These patterns, along with consistent dynamical signatures observed of the transient waves, show the sources of transient stratospheric planetary waves to clearly lie in the troposphere. Strong equatorward wave train propagation in the stratosphere is observed in early, but not in late, winter, consistent with changes in refractive index calculated for eastward-moving planetary waves, and also with changes in observed coherent mean flow variations.

ACKNOWLEDGMENTS

The authors thanks Dr David Karoly and an anonymous reviewer for constructive comments on an earlier version of this paper. Dr Karoly also provided a listing of stationary waves from the Australian climatology.

REFERENCES

Andrews, D. G. 1987 On the interpretation of the Eliassen–Palm flux divergence. *Q. J. R. Meteorol. Soc.*, **113**, 323–338

Andrews, D. G., Holton, J. R. and Leovy, C. B. 1987 *Middle atmosphere dynamics*. Academic Press

Baumhefner, D. P. 1984 The relationship between present large-scale forecast skill and new estimates of predictability error growth. Pp. 169–180 in *Predictability of fluid motions*, AIP Conference Proceedings # 106. American Institute of Physics

Barnett, J. J. and Corney, M. 1985 Middle atmosphere reference model derived from satellite data. Pp. 47–85 in *Middle atmosphere program, Handbook for MAP*, Vol. 16

Chen, S.-C. and Trenberth, K. E. 1988 Forced planetary waves in the Northern Hemisphere winter: Wave-coupled orographic and thermal forcings. *J. Atmos. Sci.*, **45**, 682–704

Dunkerton, T., Hsu, C.-P. F. and McIntyre, M. E. 1981 Some Eulerian and Lagrangian diagnostics for a model stratospheric warming. *ibid.*, **38**, 819–843

Edmon, H. J. Jr., Hoskins, B. J. and McIntyre, M. E. 1980 Eliassen–Palm cross-sections for the troposphere. *ibid.*, **37**, 2600–2616

Farrara, J. D. and Mechoso, C. R. 1986 An observational study of the final warming in the Southern Hemisphere stratosphere. *Geophys. Res. Lett.*, **13**, 1232–1235

Fraedrich, K. and Lutz, M. 1987 A modified time–longitude diagram applied to 500 mb heights along 50° north and south. *Tellus*, **39A**, 25–32

Gao, X.-H, Yu, W.-B. and Stanford, J. L. 1987 Global features of the semiannual oscillation in stratospheric temperatures and comparison between seasons and hemispheres. *J. Atmos. Sci.*, **44**, 1041–1048

Geller, M. A., Wu, M.-F. and Gelman, M. E. 1983 Troposphere–stratosphere (surface 55 km) monthly winter general circulation statistics for the Northern Hemisphere—four-year averages. *ibid.*, **40**, 1334–1352

Geller, M. A. and Wu, M.-F. 1987 Troposphere–stratosphere general circulation statistics. In *Transport processes in the middle atmosphere*. D. Reidel

Gelman, M. E., Miller, A. J., Johnson, K. W. and Nagatani, R. M. 1986 Detection of long-term trends in global stratospheric temperature from NMC analyses derived from NOAA satellite data. *Adv. Space Res.*, **6**, No. 10, 17–26

Hansen, A. R. and Sutera, A. 1986 On the probability density distribution of planetary-scale atmospheric wave amplitude. *J. Atmos. Sci.*, **43**, 3250–3265

Hartmann, D. L.	1976	The structure of the stratosphere in the Southern Hemisphere during late winter 1973 as observed by satellite. *ibid.*, **33,** 1141–1154
	1977	Stationary planetary waves in the Southern Hemisphere. *J. Geophys. Res.*, **82,** 4930–4934
Hartmann, D. L., Mechoso, C. R. and Yamazaki, K.	1984	Observations of wave–mean flow interaction in the Southern Hemisphere. *J. Atmos. Sci.*, **41,** 351–361
Hirota, I., Hirooka, T. and Shiotani, M.	1983	Upper stratospheric circulations in the two hemispheres observed by satellites, *Q. J. R. Meteorol. Soc.*, **109,** 443–454
Hitchman, M. H., Leovy, C. B., Gille, J. C. and Baily, P. L.	1987	Quasi-stationary zonally asymmetric circulations in the equatorial lower mesosphere. *J. Atmos. Sci.*, **44,** 2219–2236
Holton, J. R. and Wehrbein, W. M.	1980	The role of forced planetary waves in the annual cycle of the zonal mean circulation of the middle atmosphere. *ibid.*, **37,** 1968–1983
James, I. N.	1988	On the forcing of planetary scale Rossby waves by Antarctica. *Q. J. R. Meteorol. Soc.*, **114,** 619–637
Jenkins, G. M. and Watts, D. G.	1968	*Spectral analyses and its applications.* Holden-Day
Karoly, D. J.	1985	An atmospheric climatology of the Southern Hemisphere based on ten years of daily numerical analyses (1972–83): II. Standing wave climatology. *Aust. Meteorol. Mag.*, **33,** 105–116
	1987	The impact of base-level analyses on stratospheric circulation statistics for the Southern Hemisphere. *Pageoph.* (in press)
Knittle, J.	1976	Ein Beitrag zur Klimatologie der Stratosphäre der Südhalbkugel. *Meteorol. Abh. Meteorol. Inst., Berlin,* **A2,** (No. 1)
Labitzke, K. and van Loon, H.	1972	'The stratosphere in the Southern Hemisphere'. In *Meteorology of the Southern Hemisphere,* Meteorol. Monogr., American. Meteorological Society
Lau, N.-C.	1988	Variability of the observed midlatitude cyclone tracks in relation to low-frequency changes in the circulation patterns. *J. Atmos. Sci.* (in press)
Marks, C. J.	1988	Linear wavetrains in models of the stratosphere. *Q. J. R. Meteorol. Soc.*, **114,** 297–323
Mechoso, C. R., Hartmann, D. L. and Farrara, J. D.	1985	Climatology and inter-annual variability of wave, mean-flow interaction in the Southern Hemisphere. *J. Atmos. Sci.*, **42,** 2189–2206
Newman, P. A.	1986	The final warming and polar vortex disappearance during the Southern Hemisphere spring. *Geophys. Res. Lett.*, **13,** 1228–1231
Newman, P. A. and Randel, W. J.	1988	Coherent ozone-dynamical changes in the Southern Hemisphere spring, 1979–1986. *J. Geophys. Res.*, in press
O'Neill, A. and Youngblut, C. E.	1982	Stratospheric warmings diagnosed using the transformed Eulerian-mean equations and the effect of the mean state on wave propagation. *J. Atmos. Sci.*, **39,** 1370–1386
Palmer, T. N.	1981	Aspects of stratospheric sudden warmings studied from the transformed Eulerian-mean viewpoint. *J. Geophys. Res.*, **86,** 9679–9687
	1982	Properties of the Eliassen–Palm flux for planetary scale motions. *J. Atmos. Sci.*, **39,** 992–997
Quiroz, R. S.	1987	Traveling waves and regional transitions in blocking activity in the Northern Hemisphere. *Mon. Weather Rev.*, **115,** 919–935
Randel, W. J.	1987a	A study of planetary waves in the southern winter troposphere and stratosphere. Part I: Wave structure and vertical propagation. *J. Atmos. Sci.*, **44,** 917–935
	1987b	The evaluation of winds from geopotential height data in the stratosphere. *ibid.*, **44,** 3097–3120
	1987c	'Global atmospheric circulation statistics, 1000–1 mb.' NCAR Technical Note NCAR/TN-295 + STR
	1988	Further modification of time–longitude lag correlation diagrams: Application to three-dimensional wave propagation. *Tellus,* **40A,** 557–571

Randel, W. J., Stevens, D. E. and Stanford, J. L.	1987	A study of planetary waves in the southern winter troposphere and stratosphere. Part II: Life cycles. *J. Atmos. Sci.*, **44**, 936–949
Robinson, W. A.	1986a	The application of the quasi-geostrophic Eliassen–Palm flux to the analysis of stratospheric data. *ibid.*, **43**, 1017–1023
	1986b	The behavior of planetary wave 2 in preconditioned zonal flows. *ibid.*, **43**, 3109–3121
Shiotani, M. and Gille, J. C.	1987	Dynamical factors affecting ozone mixing ratios in the Antarctic lower stratosphere. *J. Geophys. Res.*, **92**, 9811–9824
Smith, A. R.	1983	Stationary waves in the winter stratosphere: Seasonal and interannual variability. *J. Atmos. Sci.*, **40**, 245–261
Taljaard, J. J., van Loon, H., Crutcher, H. L. and Jenne, R. L.	1969	*Climate of the upper air: Southern Hemisphere.* Vol. 1: *Temperatures, dew points and heights at selected levels.* NAVAIR-50-1C-55, Naval Weather Service Command. Washington, D.C.
Trenberth, K. E.	1980	Planetary waves at 500 mb in the Southern Hemisphere, *Mon. Weather Rev.*, **108**, 1378–1389
Trenberth, K. E. and Olson, J. G.	1988a	'Evaluation of NMC Global Analyses: 1979–1987'. NCAR Technical Note NCAR/TN-299+STR
	1988b	'Intercomparison of NMC and ECMWF global analyses: 1980–1986'. NCAR Technical Note NCAR/TN-301+STR
van Loon, H. and Jenne, R. L.	1972	The zonal harmonic standing waves in the Southern Hemisphere. *J. Geophys. Res.*, **77**, 992–1003
van Loon, H. and Labitzke, K.	1973	Zonal harmonic standing waves. *ibid.*, **78**, 4463–4471
Wakata, Y. and Uryu, M.	1987	Stratospheric multiple equilibria and seasonal variations. *J. Meteorol. Soc. Jap.*, **65**, 27–41
Yamazaki, K. and Mechoso, C. R.	1985	Observations of the final warming in the stratosphere of the Southern Hemisphere during 1979. *J. Atmos. Sci.*, **42**, 1198–1205